Chapter 22
High-Temperature Strength and Form Stability of Compact and Cellular Carbon-Bonded Alumina

Horst Biermann, Anja Weidner, and Xian Wu

22.1 Introduction

If not removed timely during the steel production, nonmetallic inclusions (NMIs) will remain in steel products and weaken their mechanical strength, resulting in economic loss or even unexpected disasters. Therefore, the reduction or elimination of NMIs becomes crucial if a high-quality steel supply must be guaranteed. Removal of NMIs by filtration before metal solidification provides an effective way to solve this problem. High-temperature filtration using ceramic foam filters (CFFs) was first applied for the purification of molten aluminum in the 1960s [1]. The rapid development of this technology in aluminum industries began in the 1970s [2, 3]. Its application to other metals followed soon [4]. Due to the much higher melting point of steel (ca. 1536 °C), the filter material for steel filtration should meet very high demands on its thermal and thermomechanical properties. As an engineering material used in functional components such as submerged entry nozzles, stoppers and sliding gates [5], carbon-bonded alumina (Al_2O_3-C) exhibits high thermal conductivity and high thermal shock resistance, which is, therefore, suitable for usage in a high-temperature environment. Its application as filter material in steel metallurgy is intensively investigated within the Collaborative Research Center (CRC) 920 at TU Bergakademie Freiberg, Germany. To characterize and understand the physical properties and (thermo)mechanical behavior, compact Al_2O_3-C specimens as well as foam and spaghetti Al_2O_3-C filters were prepared and studied. Furthermore, the applied pitch binder based on Carbores P was partly or completely replaced by an environmental-friendly binder system based on lactose and tannin. The results can

H. Biermann (✉) · A. Weidner · X. Wu
Institute of Materials Engineering, Technische Universität Bergakademie Freiberg, Gustav-Zeuner-Straße 5, 09599 Freiberg, Germany
e-mail: biermann@ww.tu-freiberg.de

C. G. Aneziris and H. Biermann (eds.), *Multifunctional Ceramic Filter Systems for Metal Melt Filtration*, Springer Series in Materials Science 337,
https://doi.org/10.1007/978-3-031-40930-1_22

be used to evaluate the mechanical performance of the materials at room and high temperatures which are required for further optimization of filter design.

22.2 Al_2O_3-C Based on the Carbores P Binder

22.2.1 Manufacture

Compact Al_2O_3-C

The composition of raw materials was based on the formulations reported by Emmel et al. [6]. The main components consisted of α-alumina, Carbores P, carbon black and graphite. The modified pitch Carbores P served not only as the binder but also a carbon source since it remained as carbon residue after pyrolysis. A typical raw material formulation (solid part) is shown in Table 22.1.

Either granules or powders were needed for the later pressing process. Granules were obtained by mixing the raw materials in an automatic mixer equipped with two metallic stirrers for 5 min followed by adding water and glycerol [7]. Subsequently, the granules were dried in an oven to reduce the moisture content. The dried granules were then ready for pressing. In comparison, powders were derived from a slurry produced by mixing the raw materials and additives in water for 24 h in a mill with corundum balls followed by drying, grinding and sieving [8, 9]. The granules or powders were pressed uniaxially or isostatically by a pressing machine under 100–150 MPa using cylindrical or rectangular molds. After this shaping process, a thermal treatment (coking) of the pressed specimens up to 800 or 1400 °C resulted the final products. Compact cylinders were obtained alternatively by drilling from compact bars after coking. Figure 22.1 gives an overview on the pressing routes of preparing cylindrical and rectangular compact Al_2O_3-C specimens.

Cellular Al_2O_3-C

For the manufacture of cellular Al_2O_3-C filters, the above-mentioned pressing routes can certainly not be applied. Al_2O_3-C foam filters—the mostly investigated filter type

Table 22.1 An example of raw material formulation (solid part)

Component	Commercial name	Content (wt%)
α-alumina	Martoxid MR 70	66
Modified pitch	Carbores P	20
Carbon black	Luvomaxx N-991	6
Graphite	AF 96/97	8
Total		**100**

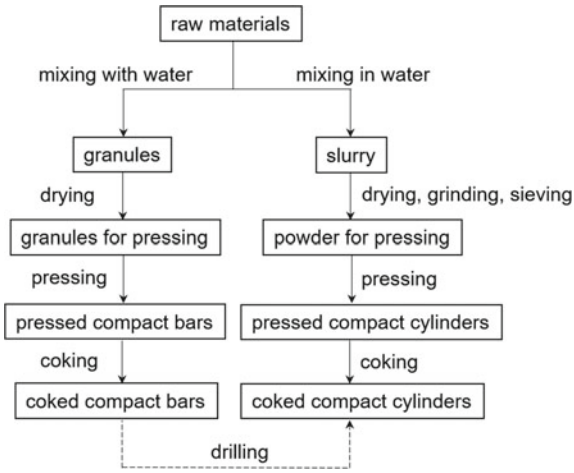

Fig. 22.1 The pressing routes (granule route on the left and slurry route on the right) for production of cylindrical and rectangular compact Al_2O_3-C

under CRC 920—were prepared through the replica method. Invented independently by Schwartzwalder and Somers as well as Holland in 1963 [1, 10], the replica method is currently widely used for the manufacture of CFFs [6]. To prepare a cylindrical Al_2O_3-C foam filter, a polyurethane foam with a defined geometry and ppi (pores per inch) parameter was used as the template. This was impregnated with the Al_2O_3-C slurry. After drying, the foam surface was sprayed with another slurry with the same composition but different viscosity (i.e. different water content). After drying again, the polymer scaffold was burned out by thermal treatment (up to 800 or 1400 °C). Thus, the replicated ceramic foam was obtained which was either used as the final product or was coated by another formulation of slurry followed by drying and thermal treatment. The corresponding products were assigned as uncoated or coated Al_2O_3-C foam filters, respectively.

Spaghetti filters were manufactured by alginate-based robo gel casting [11]. An alginate-containing Al_2O_3-C slurry was prepared and added into an alkaline earth (calcium or barium) salt solution through a nozzle. The movement of the nozzle was guided and controlled by a robot system. Thus, a stacked spaghetti plate was generated which became stiff after gelation triggered by chelation between the alkaline earth metal ions and the alginate chains. The stiff cast was then removed from the solution and dried. After thermal treatment (up to 800 °C), a coked Al_2O_3-C plate in spaghetti form was obtained. Cylinders for mechanical tests were then cut from the plate. Figure 22.2 gives an overview of the preparation routes to cellular Al_2O_3-C.

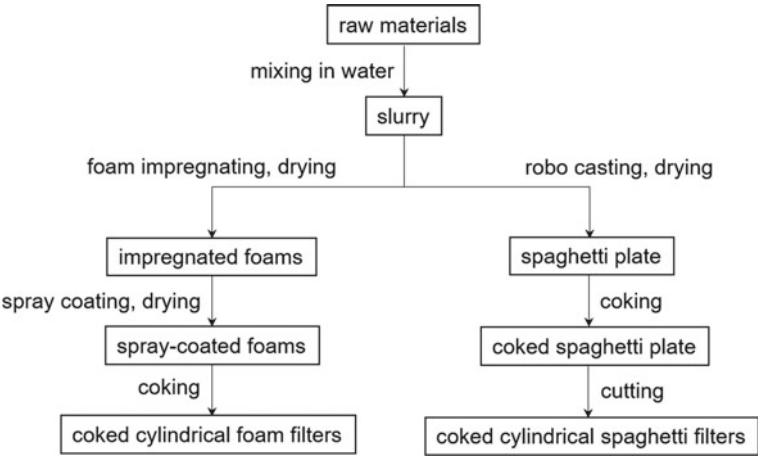

Fig. 22.2 The replica route (left) and the robo gel casting route (right) for production of Al_2O_3-C foam and spaghetti filters

22.2.2 Physical and Microstructural Properties

Compact Al_2O_3-C

Klemm et al. prepared compact Al_2O_3-C initially via the granule route [7]. Cylinders (Ø 50 mm and 50 mm height) and bars (7 mm × 7 mm × 70 mm) were obtained by uniaxial as well as isostatic pressing, followed by coking at 800 °C. To explore the influence of the binder amount, specimens with Carbores P content ranging from 5 to 30 wt% were prepared. It was found that the bulk density of the specimens decreased with the Carbores P content (ca. 1.93 g/cm^3 at 5 wt% Carbores P vs. ca. 1.84 g/cm^3 at 30 wt% Carbores P) (Fig. 22.3a). The corresponding open porosity decreased with increasing Carbores P content which reached a minimum (ca. 29.5%) at 20 wt% Carbores P and increased again at 30 wt% Carbores P (Fig. 22.3b). The degree of volume shrinkage after thermal treatment showed a similar trend with a maximum of ca. 3.6% at 20 wt% Carbores P. Substitution of the coarse-grained Carbores P with a particle size of d_{50} = 80 µm by a fine-grained variant (d_{50} = 5 µm) at 15 wt% binder content led to an increase in open porosity and decreases in bulk density (Fig. 22.3a and b). Above 15 wt% binder content, uniaxially pressed specimens showed higher open porosity and lower bulk density in comparison to specimens made by isostatic pressing. The volume shrinkage was generally stronger for uniaxially pressed specimens.

Compact Al_2O_3-C cylinders and bars of the same sizes were also prepared via the slurry route [8, 9]. The specimens were shaped by uniaxial pressing and coked at either 800 or 1400 °C. A comparison of two sticks made by the granule and slurry route, respectively, showed that the macrostructure of the former was rougher [9]. Even cracks were found between granules due to the high strength of these. Coking at

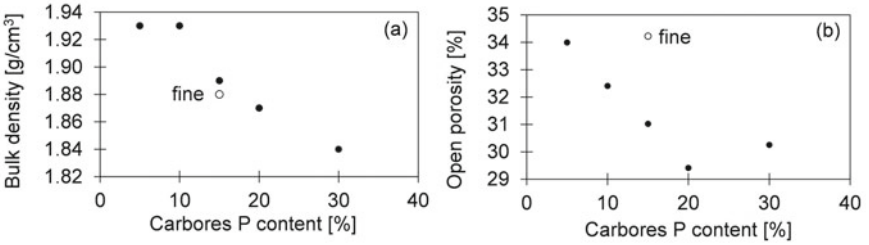

Fig. 22.3 Open porosity **a** and bulk density **b** of compact Al_2O_3-C specimens made by the granule route [7]

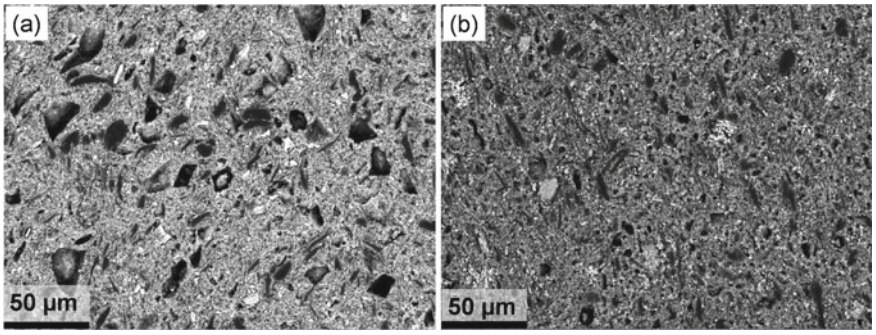

Fig. 22.4 SEM images of compact specimens with 10 wt% binder made by the slurry route: **a** coked at 800 °C; **b** coked at 1400 °C

1400 °C instead of 800 °C led to lower open porosity, stronger shrinkage and higher bulk density since higher temperature favors compaction of the microstructure [8]. A comparison of the scanning electron microscopy (SEM) images of the microstructure of specimens with 10 wt% binder coked at 800 and 1400 °C indicated that the binder residue of the latter had smaller grain sizes (Fig. 22.4).

Cellular Al_2O_3-C

Ranglack-Klemm et al. reported the preparation of carbon nanotubes/alumina nanosheets (CNT-ANS) or alumina nanospheres (CNT-ANB) coated Al_2O_3-C foam filters with 20 wt% Carbores P in cylindrical form (10 ppi, Ø 20 mm and 25 mm height) [12]. Compared with the uncoated Al_2O_3-C foam filters, the coated ones exhibited slightly higher open microporosity and comparable residual carbon content.

Studies were also carried out on Al_2O_3-C-coated as well as Al_2O_3-coated Al_2O_3-C foam filters (20 wt% Carbores P, Ø 20 mm and 25 mm height, 10 ppi) [13]. The results of mercury intrusion porosimetry showed trimodal or multimodal distribution patterns of the specimens with similar open microporosity (ca. 35%). A further

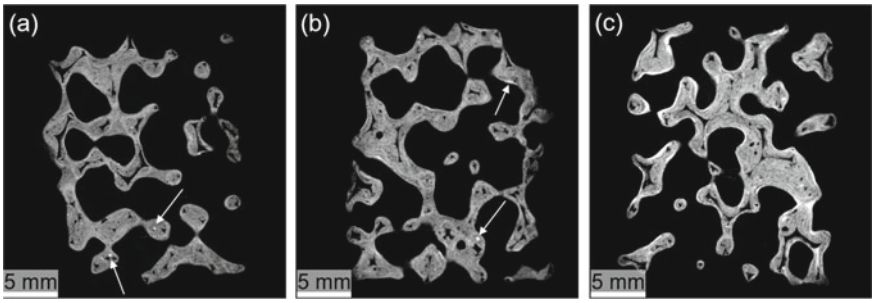

Fig. 22.5 Reconstructed CT images of Al_2O_3-C foam filters: **a** uncoated; **b** coated with Al_2O_3-C; **c** coated with Al_2O_3 [13]

examination by computer tomography (CT) revealed higher macroporosity of the Al_2O_3-coated specimen than that of the Al_2O_3-C-coated one (64 vs. 60%), although the total porosity was almost the same (70%). The CT images also revealed the inhomogeneous distribution of alumina coating (Fig. 22.5). The arrows indicate some bright spots as examples of inhomogeneously distributed alumina.

22.2.3 Mechanical and Thermomechanical Behavior

Mechanical tests were performed on Al_2O_3-C compact specimens (cylinders and bars) as well as Al_2O_3-C foam and spaghetti filters at room and high temperatures. Room temperature tests were carried out under air atmosphere. High-temperature tests were carried out between 700 and 1500 °C. To avoid the oxidation of carbon, it was necessary to run the tests under a protective atmosphere. A specially designed high-temperature testing machine equipped with a sealable chamber and argon supply could meet such a requirement. The specimens were heated by electromagnetic induction in both compression (for cylindrical specimens) and bending (for rectangular specimens) modes. Figure 22.6 shows the machine and the experimental setup for testing cylindrical foam filters. Susceptors made by TZM (titanium-zirconium-molybdenum alloy) were used to enable a homogeneous temperature distribution. More details about the testing machine and testing parameters can be found in the corresponding references [12, 13].

Compact Al_2O_3-C

Compression Behavior

Compression tests at room temperature on uniaxially pressed cylindrical specimens (Ø 50 mm and 50 mm height, coked at 800 °C) made through the granule route showed

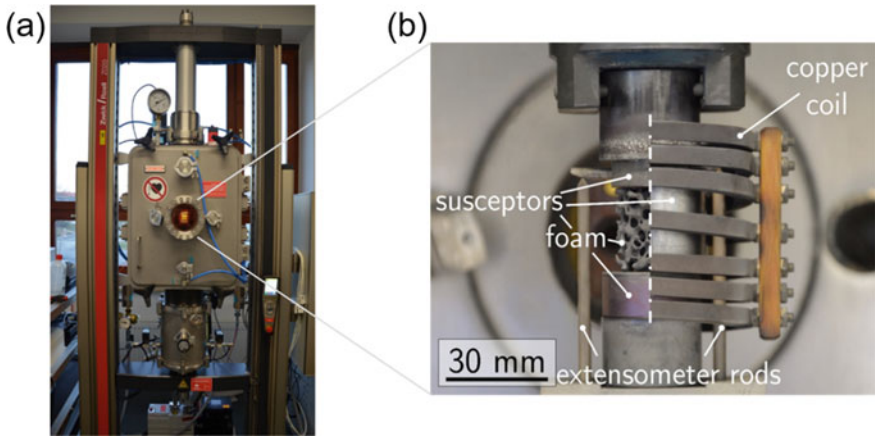

Fig. 22.6 **a** High-temperature testing machine; **b** Experimental setup for testing a foam filter at high temperatures [13]

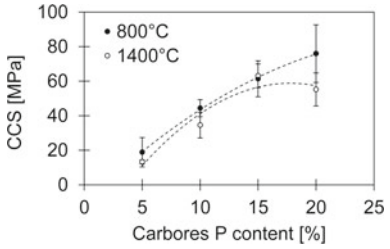

Fig. 22.7 Cold crushing strength of compact Al_2O_3-C specimens made by the slurry route coked at 800 and 1400 °C [8]

an increase of cold crushing strength (CCS) with the content of Carbores P from 5 wt% (15 MPa) to 20 wt% (44 MPa) and a slight decrease at 30 wt% (42 MPa) [7]. The CCS values of the specimens from the slurry route under otherwise comparable conditions were higher (e.g. 76 MPa vs. 44 MPa at 20 wt% Carbores P) [8]. For the specimens made by the slurry route, those coked at 1400 °C usually exhibited lower CCS than those at 800 °C (Fig. 22.7). At 20 wt% Carbores P, in particular, the difference of CCS reached the highest value of 25 MPa. Therefore, a higher coking temperature did not result in a higher CCS.

Solarek et al. investigated compression behaviors of compact Al_2O_3-C cylinders (ca. Ø 25 mm and 25 mm height) at room and high temperatures until 1500 °C [14]. The specimens were shaped by uniaxial pressing and coked at 1400 °C. A pronounced hysteresis of the compressive stress–strain curve at room temperature because of plasticization in the carbonaceous matrix was observed (Fig. 22.8). The width of the hysteresis decreased at the second loading.

Creep tests showed an increase in creep rate above 1050 °C (Fig. 22.9) and a power law was proposed to correlate stress (σ) and strain rate at 30 min ($\dot{\varepsilon}_{30\text{min}}$) (Eq. 22.1). At 750 and 1050 °C, the stress exponent n was nearly zero. At 1350 °C, n was 2.3. The activation energy of creep above 1150 °C was determined as 263 kJ/mol.

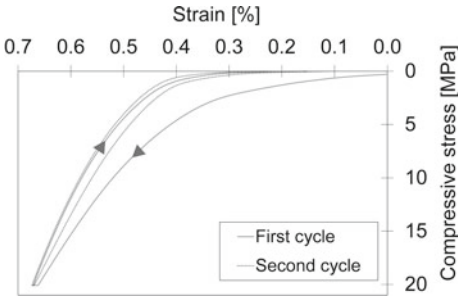

Fig. 22.8 Compressive stress–strain curves of compact Al_2O_3-C produced by uniaxial pressing at room temperature [14]

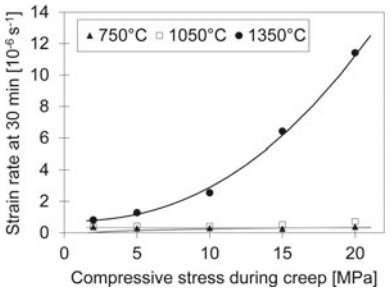

Fig. 22.9 Creep rate of compact Al_2O_3-C cylinders produced by uniaxial pressing at 750, 1050 and 1350 °C [14]

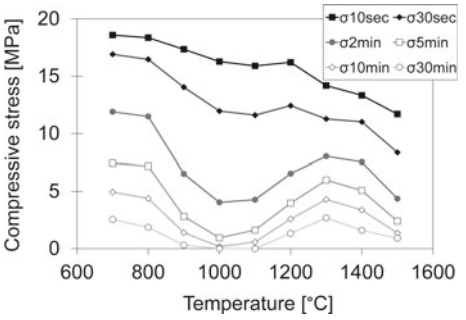

Fig. 22.10 Relaxation stress of uniaxially pressed compact Al_2O_3-C cylinders after different times at different temperatures [14]

$$\dot{\varepsilon}_{30\text{min}} \sim \sigma^n \tag{22.1}$$

Stress relaxation tests showed a minimum remaining stress between 900 and 1200 °C as well as a higher remaining stress between 1300 and 1400 °C (Fig. 22.10). During cyclic stress relaxation, stress relaxation decreased with ongoing cycling. The relatively smaller scatter supported the assumption that high-temperature deformation depends on a plastic process rather than on the size of the major defect [14].

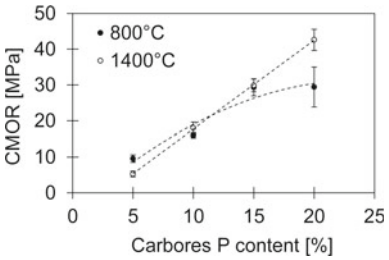

Fig. 22.11 Cold modulus of rupture of compact Al_2O_3-C specimens made by the slurry route coked at 800 and 1400 °C [8]

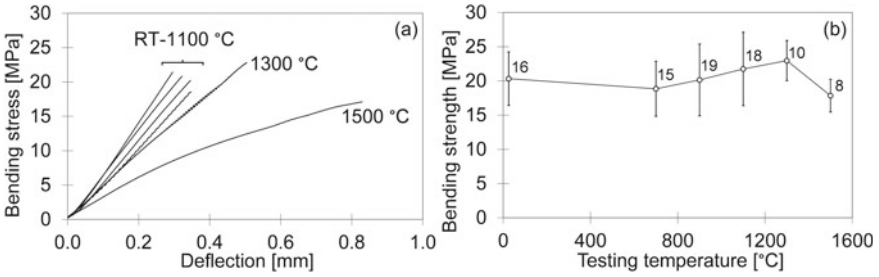

Fig. 22.12 Results of bending tests of compact Al_2O_3-C bars produced by uniaxial pressing at different temperatures: **a** stress–deflection curves; **b** bending strength versus temperature with the quantity of specimens tested at each temperature [15]

Bending Behavior

Bending tests at room temperature on granule route specimens (7 mm × 7 mm × 70 mm, uniaxially pressed, coked at 800 °C) showed that the cold modulus of rupture (CMOR) values at 20 wt% and 30 wt% Carbores P (17 MPa and 18 MPa) were significantly higher than those at 5–15 wt% Carbores P (<11 MPa) [7]. The corresponding slurry route specimens exhibited higher CMOR which reached 29 MPa at 20 wt% Carbores P [8]. Furthermore, uniaxially pressed specimens showed higher CMOR values than isostatically pressed ones, especially when the Carbores P content was above 15 wt% (Fig. 22.11) [9]. In contrast to the results of CCS values obtained by compression tests, the CMOR value was found higher at 20 wt% Carbores P for specimens coked at 1400 °C than that of 800 °C (42 MPa vs. 28 MPa) [8]. Therefore, a higher coking temperature led to higher bending strength.

Solarek et al. studied the bending behavior of larger compact bars (ca. 25 mm × 25 mm × 145 mm, uniaxially pressed, coked at 1400 °C) at room and high temperatures up to 1500 °C (Fig. 22.12) [15]. A maximum bending strength value was recorded at 1300–1400 °C which could be explained by changes of the material behavior from brittle to ductile leading to reductions in stress concentrations.

In contrast, bending tests on pure graphite bars did not show any softening up to 1500 °C and the strength increased with the temperature [15]. Such differences between graphite and carbon-bonded alumina might result from the higher thermal expansion of alumina in comparison to carbon. Thus, the generated compressive stresses within the graphitic layers of the carbonaceous matrix could promote the glide of the layers already far below 2000 °C. Moreover, they could enhance fracture toughness by closing cracks and increasing resistance against crack growth [15].

Fracture Mechanical Behavior

Compact bars (ca. 25 mm × 25 mm × 145 mm, uniaxially pressed, coked at 1400 °C) were further tested on single edged V-notched beams at room and high temperature [16]. With help of an optical system, the crack mouth opening displacement (CMOD) was measured precisely. Typical force-CMOD-curves of the material are shown in Fig. 22.13.

At room temperature, the force dropped immediately to zero at very small CMOD (30 μm) after a linear-elastic deformation at the beginning. The specimen behaved brittle with instable crack propagation and low work of fracture at room temperature. The fracture toughness K_{Ic} was determined as 0.69 ± 0.07 MPa · $m^{1/2}$. At 1400 °C, the material became ductile and visco-plastic and showed, compared to the result at room temperature, a significant increase of toughness and work of fracture, although a quantitative analysis of the latter was not possible due to large scatter of the CMOD signal. Macroscopic deformation as well as cracks arising from temperature gradients during cooling were observed on specimens after testing at 1400 °C [16].

Cellular Al_2O_3-C

Solarek et al. performed compression tests on uncoated foam filters (coked at 1400 °C) at 800–1500 °C [15]. Similar to the results of bending tests on compact

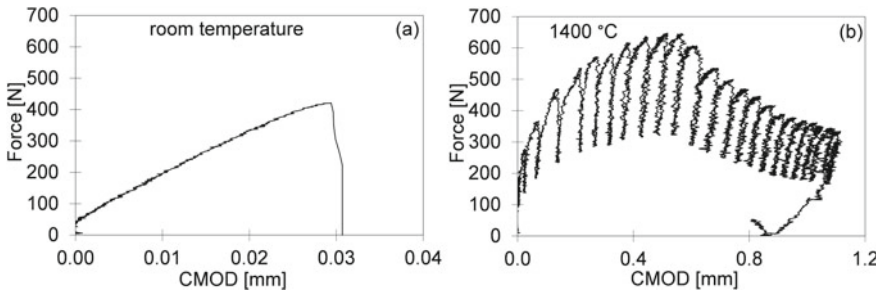

Fig. 22.13 Typical force-CMOD-curves of Al_2O_3-C: **a** at room temperature; **b** at 1400 °C with unloading steps [16]

bars of the same material, the foam filters exhibited a maximum strength value at 1300–1400 °C, indicating again a brittle-to-ductile transition. Furthermore, the force–displacement curves at temperatures below 1200 °C indicated ruptures of individual foam struts (see the arrows in Fig. 22.14a). At 1400 and 1500 °C, the curves showed fewer loading drops and became smoother, obviously due to significant plastic deformation (Fig. 22.14b). It was supposed that the presence of an electromagnetic field supports the formation of graphitic structures, which was observed using Raman spectroscopy (Fig. 22.15).

Selected specimens after compression tests were examined by SEM in secondary electron mode (Fig. 22.16). Numerous failed foam struts were observed at temperatures not exceeding 1300 °C (Fig. 22.16a). No plastic deformation was visible. Figure 22.16b shows a specimen that was 2 mm shortened after testing at 1500 °C with a partly cracked foam strut at the lower center (Fig. 22.16c).

Ranglack-Klemm et al. investigated the compression behavior of Al_2O_3-C foam filters without and with functional coatings of CNT-ANS or CNT-ANB (see Sect. 2.2.2) at 1100 °C and 1450 °C [12]. The application of functional coatings led to higher compressive strength at 1100 °C with the highest performance achieved by the CNT-ANS coating. The study showed also the brittle character of the filter materials at 1100 °C which turned into viscoplastic behavior with pronounced plastic deformation at 1450 °C (Fig. 22.17).

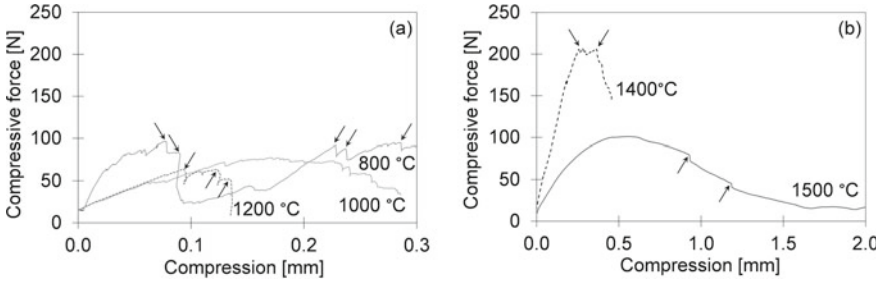

Fig. 22.14 Force-compression curves of Al_2O_3-C foams: **a** at 800, 1000 and 1200 °C; **b** at 1400 and 1500 °C [15]

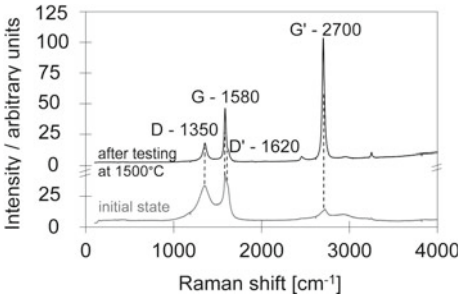

Fig. 22.15 Raman spectra of Al_2O_3-C foams before (gray) and after compression test at 1500 °C (black) [15]

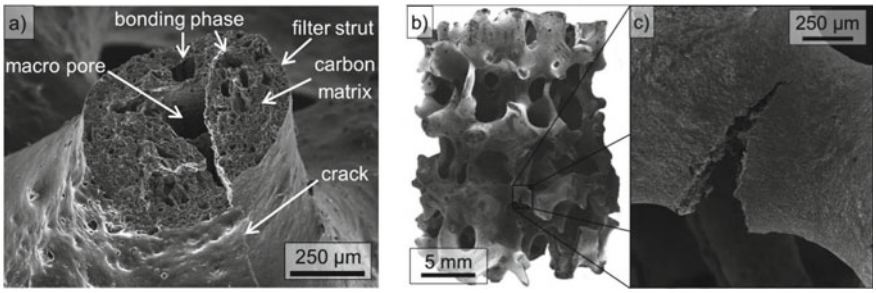

Fig. 22.16 SEM micrographs of Al_2O_3-C foams after compression tests **a** at room temperature and **b**, **c** at 1500 °C [15]

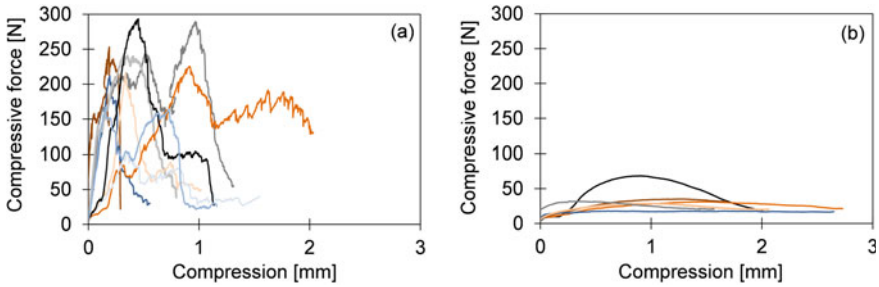

Fig. 22.17 Compressive force-strain curves of Al_2O_3-C foams coated with CNT-ANS tested at **a** 1100 °C and **b** 1450 °C [12]

Compression tests on uncoated, Al_2O_3-C-coated or Al_2O_3-coated Al_2O_3-C foam filters at 1300, 1400 and 1500 °C showed that the coated specimens were more resistant against compression [13]. While brittle behavior was dominant at 1300 °C, the transition from brittle to viscoplastic deformation became apparent at 1400 °C and 1500 °C (Fig. 22.18). Figure 22.19 shows the compressive strength and the corresponding compression values of the uncoated and coated filters tested at 1300, 1400 and 1500 °C. Despite high scatter, the filters coated with Al_2O_3-C (coating 1) exhibit the smallest compressive strength at 1400 °C. This could be explained by the softening of the carbon-containing binder phase which was highly viscous at that temperature, leading to a relatively low compressive strength. At 1500 °C, the viscosity was sufficiently low, so that healing of defects occurred, resulting in higher compressive strength.

According to the SEM analysis on Al_2O_3 coated filters, struts with spalled coating were observed after testing at 1300 °C (Fig. 22.20a). Some arrested cracks and intact coating were observed on a filter after testing at 1400 °C (Fig. 22.20b). Furthermore, a significant viscoplastic deformation led to the buckling of the coating (Fig. 22.20d). A polished section of a filter specimen showed a continuous gap between the filter (I) and the Al_2O_3 coating (II) (Fig. 22.20c). During the thermomechanical testing, this gap caused a wall-slip effect between the coating and substrate.

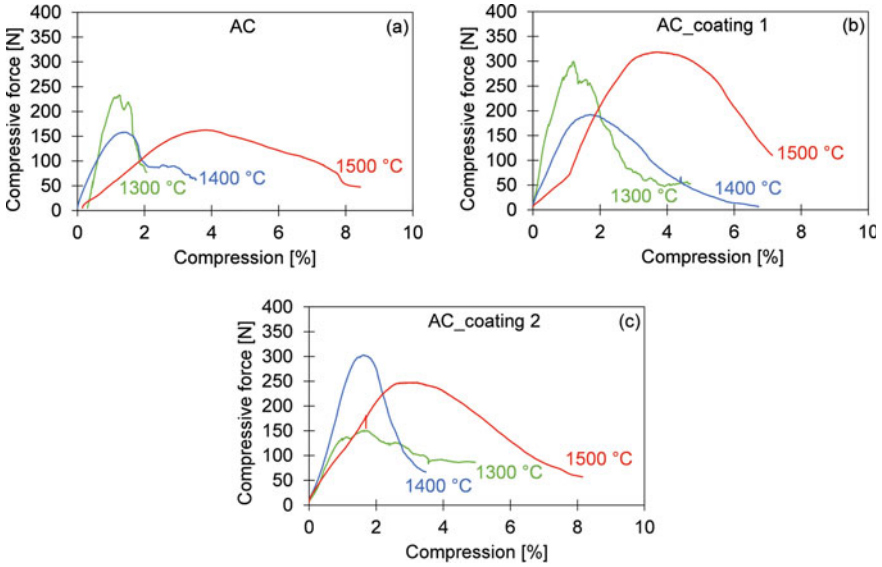

Fig. 22.18 Typical compressive force-strain curves of Al_2O_3-C (AC) foams: **a** uncoated; **b** coated with Al_2O_3-C (coating 1): **c** coated with Al_2O_3 (coating 2) [13]

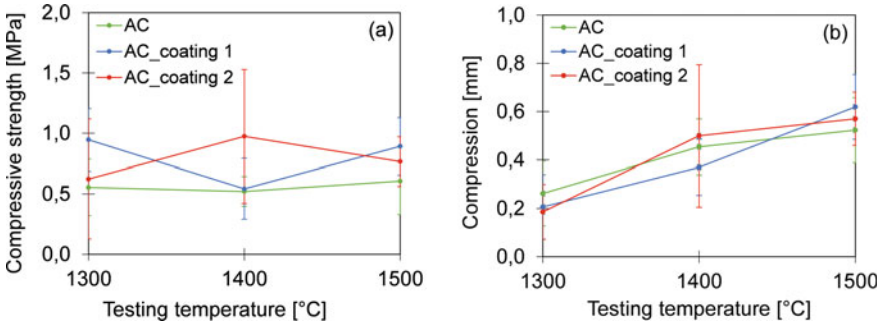

Fig. 22.19 Comparison of the values of compressive strength (**a**) and compression at maximum strength (**b**) tested at different temperatures (AC = uncoated, AC_coating 1 = coated with Al_2O_3-C, AC_coating 2 = coated with Al_2O_3) [13]

To examine the residual thermomechanical properties of Al_2O_3-C foam filters coated with carbon-containing calcium dialuminate (CA_2-C) or calcium hexaaluminate (CA_6-C) after contact with steel melt, the filters were immersed into steel melt under argon atmosphere in a metal casting simulator at 1650 °C for 10 s [17]. Compression tests were then performed on these residual filters at 1100 °C and 1500 °C (Fig. 22.21). Similar to the above-mentioned studies, the filter materials exhibited brittleness at 1100 °C and ductility at 1500 °C with considerable compression strengths at both temperatures. Hence, even after contact with steel melt, the

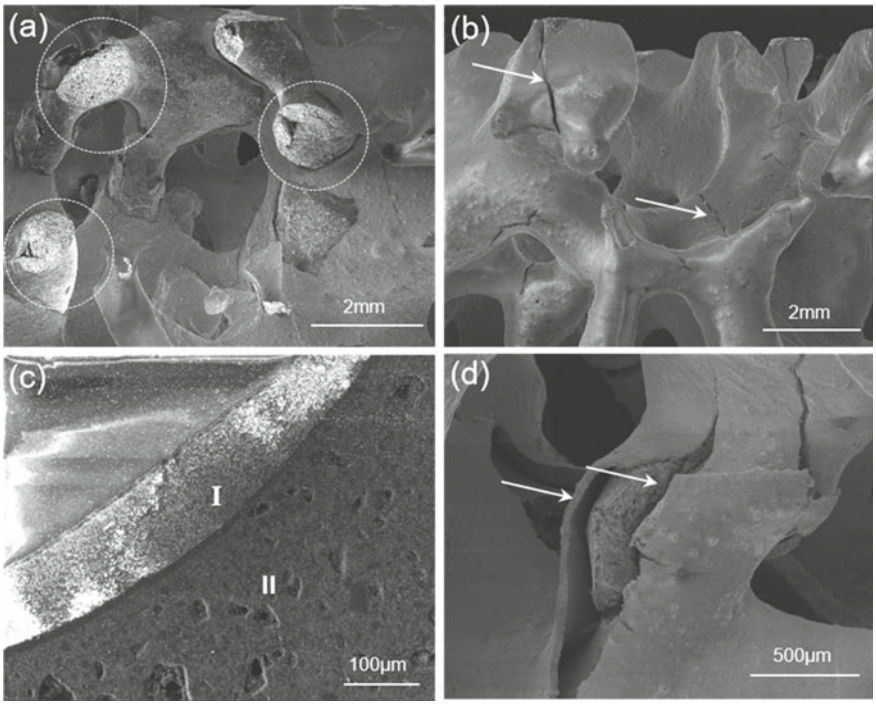

Fig. 22.20 SEM images of Al_2O_3-coated Al_2O_3-C foam filters after testing at different temperatures; **a** 1300 °C; **b** 1400 °C; **c**, **d** 1500 °C [13]

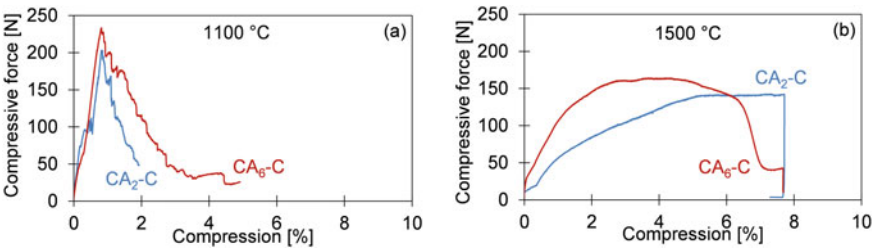

Fig. 22.21 Force-compression curves of residual filters at different temperatures: **a** 1100 °C; **b** 1500 °C [17]. Please note that the tests shown in (**b**) were interrupted shortly before 8% compression due to machine limitations

mechanical behavior of the specimens was not significantly influenced. Also, the pore size distribution and carbon content did not change much after the immersion. Energy dispersive spectroscopy (EDS) analysis of the filter coated with CA_6-C after compression test at 1100 °C showed the remaining coating material (Fig. 22.22) and some steel droplets (Fig. 22.22e).

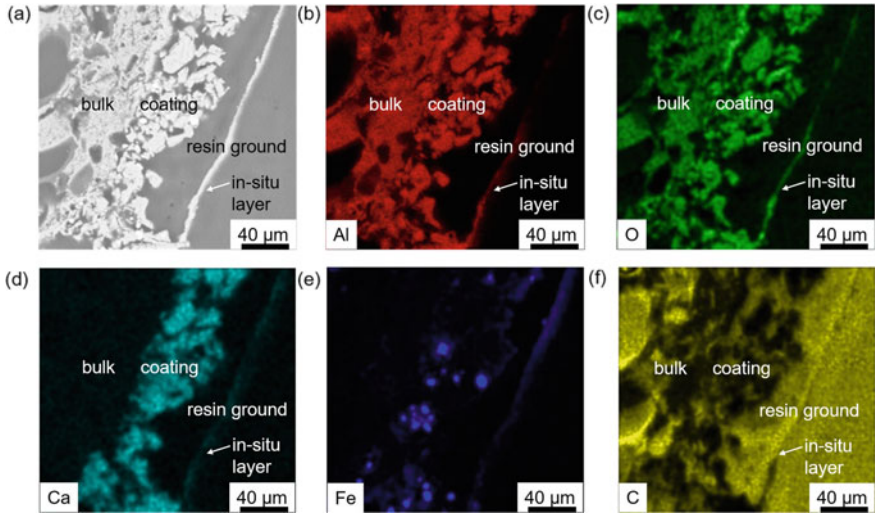

Fig. 22.22 CA_6-C-coated foam filter residue after compression test at 1100 °C: **a** back scattered electrons (BSE) micrograph; **b–f**: distribution of elements Al, O, Ca, Fe and C [17]

The compression behavior of Al_2O_3-C spaghetti filters was studied at room temperature, 800 and 1500 °C (Fig. 22.23) [18]. Ductile deformation occurred only at 1500 °C (Fig. 22.23c). In comparison to the foam filters of similar material composition and size, the spaghetti filters showed significantly higher compression strength at high temperatures. The compressive strength-density diagram of foam and spaghetti filers tested at 800 °C showed a significant difference in the regression slopes, indicating that the higher compressive strength of the spaghetti filters cannot be explained by the higher mass alone (Fig. 22.24). The full struts (not hollow as in the case of foam filters) should have a positive influence on the mechanical strength of the spaghetti filters.

22.3 Al_2O_3-C Based on the Lactose-Tannin Binder System

22.3.1 The Lactose-Tannin Binder System

Although pitch-based binders have been used for the manufacture of refractories for more than 100 years [19], one crucial drawback is the release of carcinogenic compounds such as benzo[a]pyrene during thermal treatment [20]. In the case of Carbores P, the amount of harmful substances is limited to a lower level. However, their concentration still cannot fully meet the REACH (Registration, Evaluation, Authorisation and Restriction of Chemicals) criterium in Europe [21]. Besides the pitch binders, phenolic resins are also common binders for producing carbon-bonded

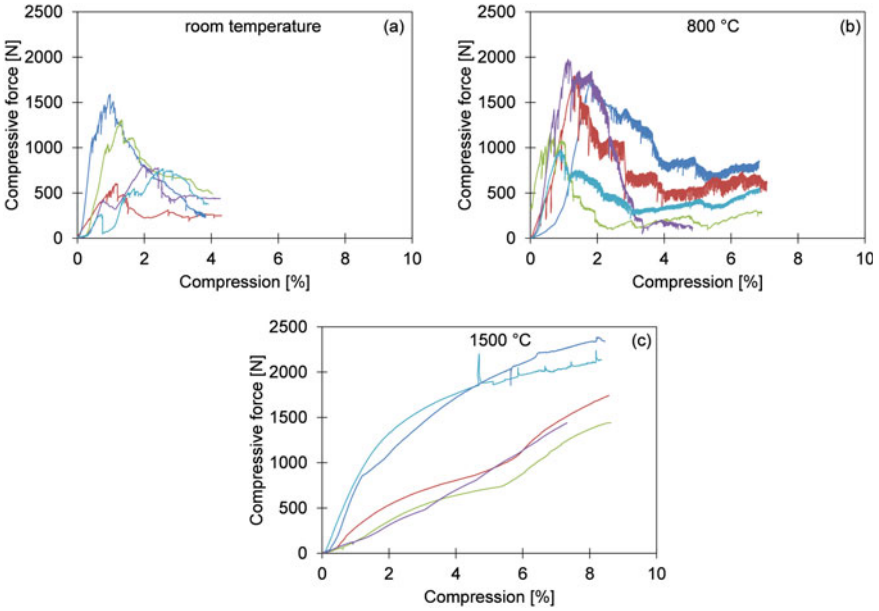

Fig. 22.23 Force-compression curves of Al_2O_3-C spaghetti filters tested at different temperatures: **a** room temperature; **b** 800 °C; **c** 1500 °C [18]

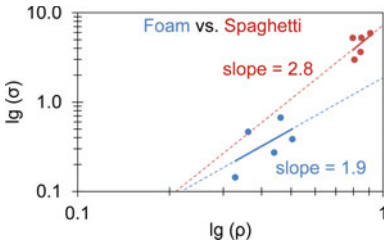

Fig. 22.24 Compressive strength-density diagram of Al_2O_3-C foam and spaghetti filters tested at 800 °C [18]

refractories [22]. Unfortunately, the production of theses resins releases free phenol which is hazardous to the environment, too [23]. Therefore, searching for alternative binder systems with environmental-friendly character is meaningful. One promising candidate is a binder system based on a combination of lactose and tannin. First attempts to use the lactose-tannin (L–T) binder system for the manufacture of MgO-C bricks and Al_2O_3-C foam filters showed positive results [24–26].

Lactose (Latin *lac* for milk + chemical suffix *-ose*) is a double sugar existing in dairy products. Cow milk, for example, contains ca. 5 wt% lactose as the second most important component after water. Lactose is a structurally well-defined substance whose chemical structure (combined with one water molecule, i.e. monohydrate) is shown in Fig. 22.25a. Lactose as a binder finds applications in pharmaceutical and food industries as well as for ore processing [27].

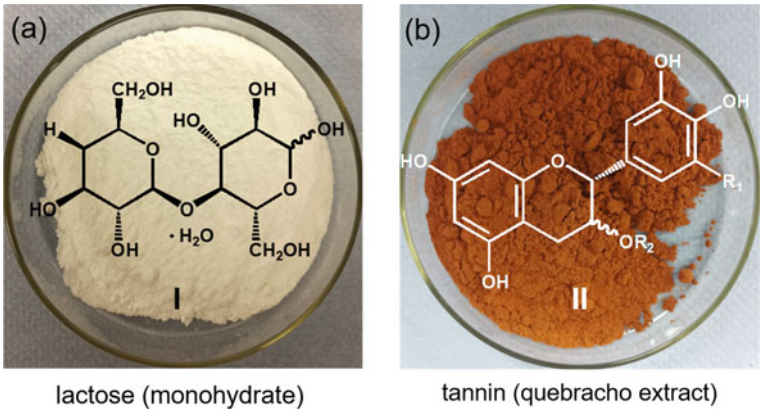

Fig. 22.25 Chemical structures and appearance of lactose (**a**) and tannin (**b**) used in our study

Tannin (from Old High German *tanna* for conifer) is a common component found in many plants such as in tree barks, leaves, stems, fruits, roots, etc. However, tannin is not a substance with a unique molecular structure, but rather a collective name for structurally different molecules which are called vegetable polyphenols. According to Freudenberg (the German chemist who was famous for his contributions to natural organic compounds), tannins are generally divided into two types: hydrolyzable and condensed tannins. Currently, most of the worldwide produced tannins are condensed tannins in which flavonoids (e.g. catechins) are the basic structural unit [28]. The molecular weights of tannins are between 500 and 3000 g/mol. The most important application of tannins is tanning animal skins into leather. The tannin used in our study is a natural condensed tannin extracted from Quebracho trees. Its basic structural fragments are catechins as shown in Fig. 22.25b.

22.3.2 Manufacture

Two strategies were applied for the formulation of the L–T-based binder system: pitch reduction [29] and pitch replacement [30]. In the first case, 80 wt% of Carbores P was replaced by lactose and tannin, i.e. the binder system consisted of 16 wt% L–T and 4 wt% Carbores P (pitch-lean L–T-based binder system). In the second case, Carbores P was completely replaced by lactose and tannin (pitch-free L–T-based binder system). In both cases, the ratio of lactose and tannin was varied systematically. Examples of raw material composition (main solid part) based on the L–T binder system (pitch-lean and pitch-free) are given in Table 22.2.

For the manufacture of L–T-based compact Al_2O_3-C specimens, a slip casting route has been developed [29]. In comparison to the pressing routes, the slip casting route is closer to the replica route for the manufacture of foam filters due to the

Table 22.2 Examples of raw material formulation (main solid part) based on the pitch-lean and pitch-free L–T binder system

Component	Commercial name	Content (wt%)
Example formulation based on the pitch-lean L–T binder system		
α-alumina	Martoxid MR 70	66
Lactose/tannin	Mivolis Milchzucker/Quebracho-Extrakt	16
Modified pitch	Carbores P	4
Carbon black	Luvomaxx N-991	6
Graphite	AF 96/97	8
Total		**100**
Example formulation based on the pitch-free L–T binder system		
α-alumina	Martoxid MR 70	66
Lactose/tannin	Mivolis Milchzucker/Quebracho-Extrakt	20
Carbon black	N-991	6
Graphite	AF 96/97	8
Total		**100**

absence of high pressure during the whole process. Such a slip casting route was, however, not applied to the manufacture of L–T-based rectangular compact Al_2O_3-C bars (ca. 25 mm × 25 mm × 145 mm) since cracks appeared after the casting of the large specimens. Thus, L–T-based rectangular compact Al_2O_3-C specimens were prepared through the slurry route. Figure 22.26 gives an overview of the manufacture of L–T-based compact Al_2O_3-C cylinders and bars.

For L–T-based specimens, a hardening process was necessary before the cast or pressed specimens were sent to coking. During this process, the specimens were heated up to 180 °C in air, while individual tannin molecules were linked with each other through a hardening agent. The most common hardening agent for tannins is hexamethylenetetramine (also called hexamine or hexa) due to its good performance and low toxicity [31, 32]. The coking process was performed at 1000 °C. Coked bars were used directly for mechanical tests. Coked cylinders were machined into desired sizes which were further used as specimens for mechanical tests.

22.3.3 Physical and Microstructural Properties

Cylindrical compact Al_2O_3-C specimens based on the pitch-lean L–T-based binder system with a mass ratio of lactose and tannin ranging from 5:1 to 1:5 were prepared and studied [28]. It was found that the slurry viscosity increased with the tannin content which greatly influenced the quality of the casts. As the result, specimens with L:T = 1:1 and 1:5 could not be machined due to critical cracks appearing after coking, and specimens with L:T = 1:2 and 2:1 were highly porous. High-quality

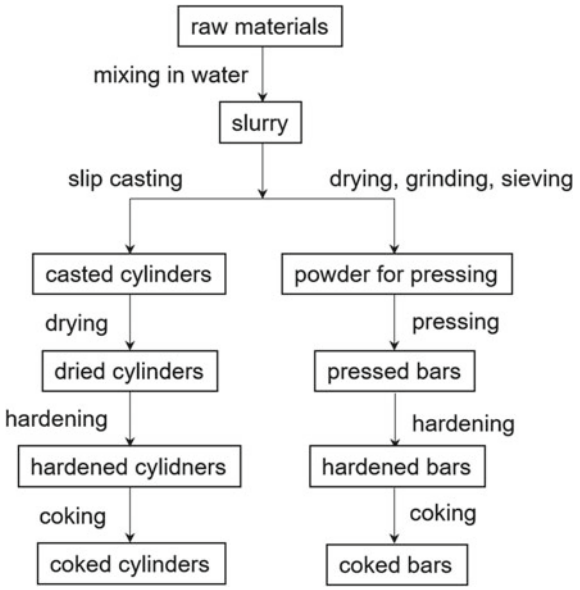

Fig. 22.26 The slip casting route for L–T-based compact Al_2O_3-C cylinders and the pressing route for L–T-based compact Al_2O_3-C bars

specimens were only producible for L:T = 5:1, 4:1 and 3:1 which showed similar volume shrinkage (5%) and mass reduction (9%) after coking and little difference in residual carbon content (23 wt%). Their bulk density and open porosity values were around 1.7 g·cm^{-3} and >40%, respectively. Furthermore, specimens with L:T = 5:1, 4:1 and 3:1 based on the pitch-free L–T binder system with comparable bulk density and porosity were prepared [30]. According to mercury intrusion porosimetry measurements, the specimens exhibited monomodal pore size distribution [30].

SEM images of the sections of coked cylindrical specimens showed all microstructural features such as alumina particles, pores and isolated carbonaceous bonding aggregates (Fig. 22.27). A microcrack was observed in the specimen with L:T = 3:1 which might be formed during thermal treatment or machining (Fig. 22.27c).

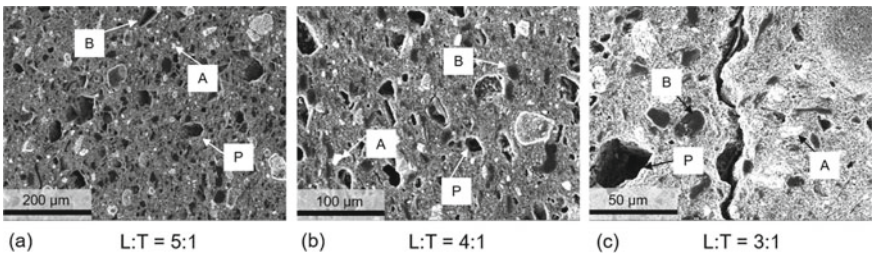

Fig. 22.27 SEM images of pitch-free L–T based compact specimens (A = alumina particle; B = isolated carbonaceous bonding aggregates; P = pore): **a** L:T = 5:1; **b** L:T = 4:1; **c** L:T = 3:1 [30]

22.3.4 Mechanical and Thermomechanical Behavior

Compression tests on cylindrical compact specimens based on the pitch-lean L–T binder system showed that the CCS values of those with L:T = 5:1 (47 MPa), 4:1 (34 MPa) and 3:1 (28 MPa) were significantly higher than L:T = 2:1 (14 MPa) and L:T = 1:2 (8 MPa) [29]. They were even higher than or comparable with the CCS value of the reference specimen (i.e. specimen based on the Carbores P binder made by slip casting) (32 MPa), although the latter exhibited higher tolerance against compression since the strain at maximum compressive stress was much higher (3–4 vs. 1–2%) as shown by the CCS test curves (Fig. 22.28). Nevertheless, the splitting tensile strength values of the L–T specimens (3–5 MPa) were much lower than that of the reference (11 MPa). This is attributed to the glassy residual carbon of the pyrolyzed L–T binders which was more fragile against tensile stress. The CCS curves of the specimens based on the pitch-free L–T binder system showed also similar character [30].

Thermomechanical tests were focused on cylindrical and rectangular compact specimens based on the pitch-free L–T binder system with L:T = 5:1, 4:1 and 3:1 [30]. High-temperature bending tests were carried out on bars (ca. 25 mm × 25 mm × 145 mm) at 700, 900, 1100, 1300 and 1400 °C (Fig. 22.29). The bending strength ranged from 0.9 to 1.6 MPa and reached generally its maximum at 1100 °C. At 1300 and 1400 °C, the specimens were more deflected. Thus, the brittle-to-ductile

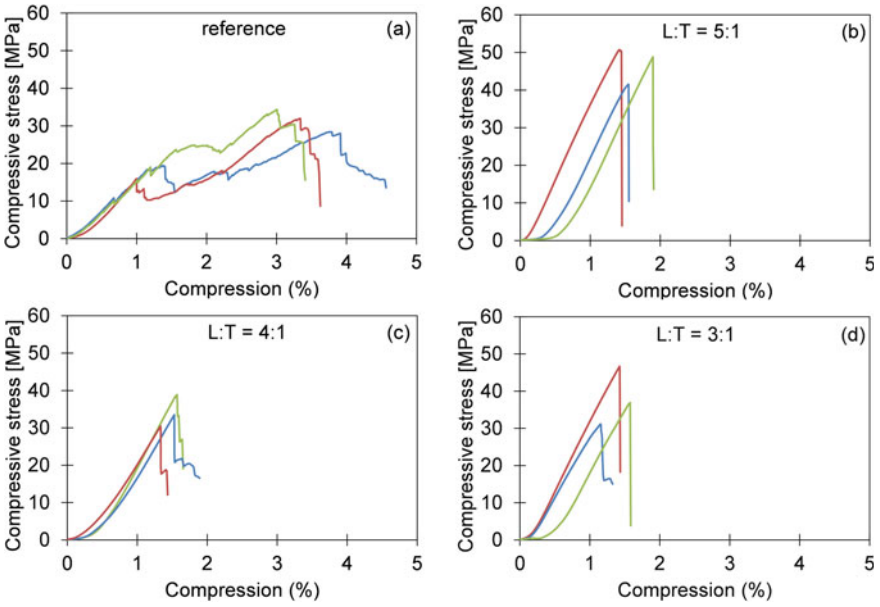

Fig. 22.28 Room temperature compression test curves: **a** pitch-based specimens; **b–d** pitch-lean L–T based specimens at different L–T ratios [29]

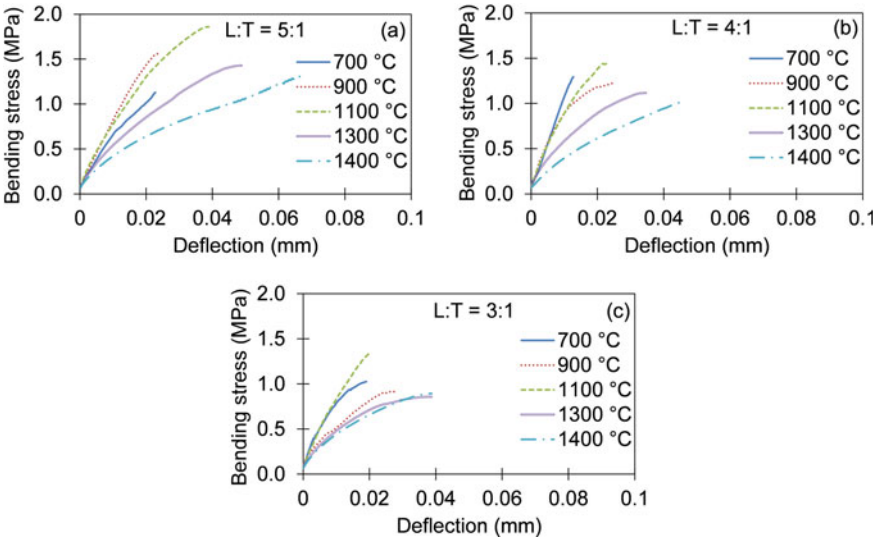

Fig. 22.29 Bending tests on pitch-free L–T-based compact specimens at high temperatures: **a** L:T = 5:1; **b** L:T = 4:1; **c** L:T = 3:1 [30]

transition should take place between 1100 and 1300 °C. L:T = 3:1 exhibited lower bending strength and lower deflection, while L:T = 5:1 showed higher deflection at 1300 and 1400 °C. The bending strengths were significantly weaker than those of the pitch-based specimens (see Fig. 22.12).

Several aspects are considered to be responsible for the observed weakness of the L–T-based bars [30]: (i) the L–T-based bars were more porous in comparison to the pitch-based ones (ca. 45% vs. ca. 37%); (ii) they contained much less residual carbon (ca. 22 wt% vs. ca. 37 wt%); (iii) the coking temperature was lower (1000 vs. 1400 °C); (iv) coking of the L–T binder system generated glassy carbon residue with higher fragility and lower deformability; (v) the hardening process might occur already at room temperature resulting in high hardness of particles which was less favorable for the pressing process.

Compression tests on small cylinders (Ø 8 mm × 12 mm) at the above-mentioned high temperatures showed that the compressive strength was between 22 and 48 MPa (Fig. 22.30). Similar to the bending tests, the maximum strength values were recorded at 1100 °C. The compressive strengths of L:T = 5:1 (23–34 MPa) were lower than those of L:T = 4:1 (38–48 MPa) and L:T = 3:1 (30–44 MPa) at the same test temperatures.

Creep tests on cylinders (Ø 20 mm × 25 mm) were performed at 1100, 1300 and 1400 °C under 10 MPa for 30 min (Fig. 22.31). While the compression values of all specimens were below 0.26% at 1100 °C, the creep effect became much more pronounced at 1300 and 1400 °C, indicating the ductility of the material at these temperatures. The compression of each specimen was even almost doubled as the temperature changed from 1300 to 1400 °C. Compared to the compositions L:T =

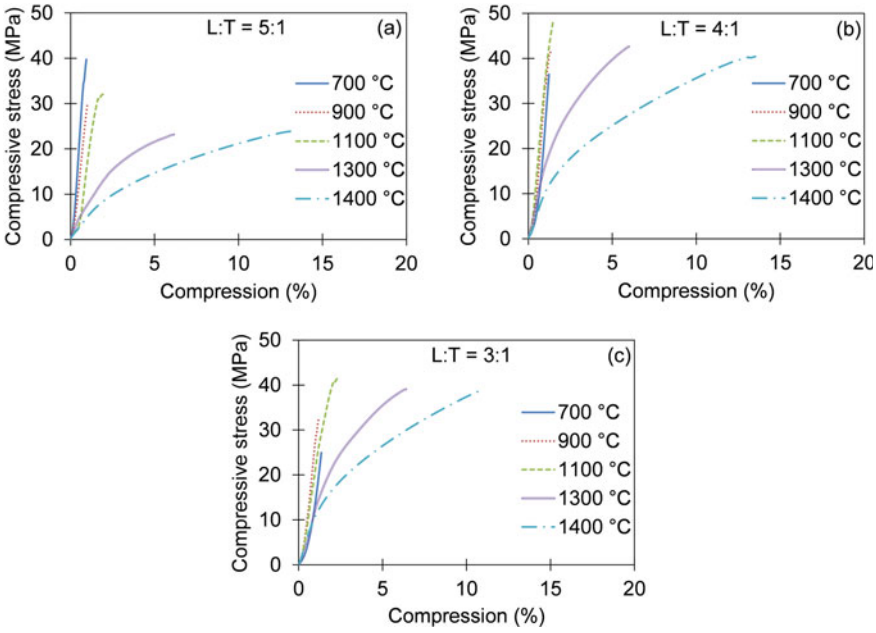

Fig. 22.30 Compression tests on pitch-free L–T-based compact specimens at high temperatures: **a** L:T = 5:1; **b** L:T = 4:1; **c** L:T = 3:1 [30]

4:1 and 3:1, the material L:T = 5:1 showed considerably higher compression at 1300 and 1400 °C.

It was also attempted to perform tests at 1500 °C [30]. As a bending bar was heated to 1500 °C, cracks appeared on the specimens unexpectedly. After cooling down, some solid grey droplets were found on the cracks. Meanwhile, some white substance was observed on test machine components. X-ray diffraction (XRD) analysis identified the grey droplets as a mixture of α-Al_2O_3, Al_2CO and C (graphite or turbostratic carbon), and the white substance as a mixture of Na_2CO_3 and NaOH. According to ball on three balls (B3B) tests as well as Raman spectroscopic investigation carried out by Zielke et al. [33], a progressive graphitization process occurred if the specimens were coked at 800 °C and tested at higher temperatures. We supposed that the sodium ions came from the commercial tannin which are not explicitly shown in its technical data sheet. The formation of the grey droplets was probably due to an overheating triggered by the electromagnetic field for induction heating and enhanced by a transition of the glassy carbon residue (deriving from L–T) into structurally more ordered form. Based on this assumption, hot spots could occur within the specimen through a synergetic interaction between a carbon modification change and an overheating. The appearance of hot spots was also observed e.g. in Field-Assisted Sintering Technology or Spark Plasma Sintering processes where a direct current is applied [34, 35]. A reference heating process up to 1500 °C using

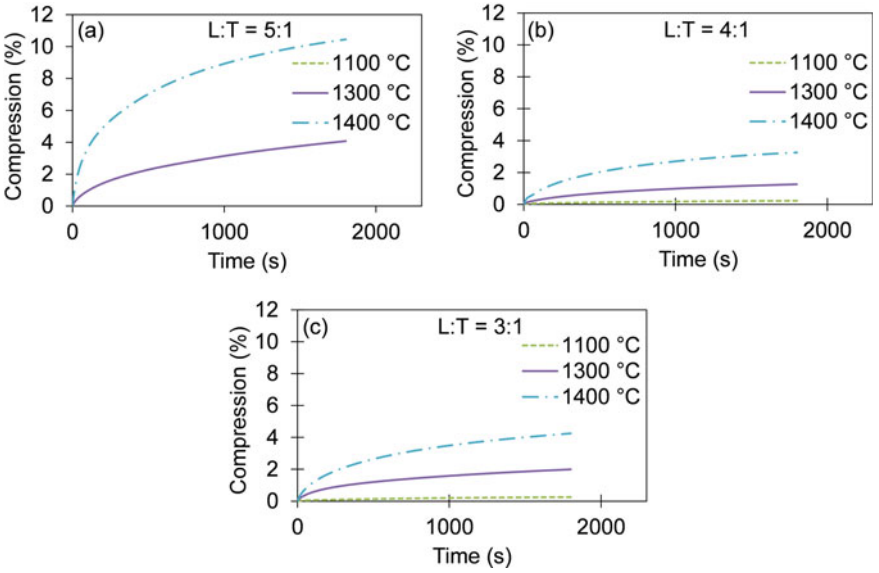

Fig. 22.31 Creep tests (10 MPa, 30 min) on pitch-free L–T-based compact specimens at high temperatures: **a** L:T = 5:1; **b** L:T = 4:1; **c** L:T = 3:1 [30]

conventional muffle oven did not lead to any visible damage on the L–T-based specimens. This supports the above-mentioned assumption. Therefore, mechanical tests on L–T-based specimens at and above 1500 °C should be carried out with resistance heating instead of inductive heating.

22.4 Summary

To characterize and further understand the physical properties and mechanical/thermomechanical behaviors of Al_2O_3-C as filter materials for molten steel, compact cylindrical and rectangular specimens as well as cylindrical foam and spaghetti filters were prepared and investigated. The application of different functional coatings on foam filters was explored. Physical parameters such as bulk density, open porosity and pore size distribution were determined. Compression and bending tests at room and high temperatures up to 1500 °C were performed. Fracture mechanical behavior was also studied. Furthermore, the modified pitch binder Carbores P was partly or completely replaced by an environmental-friendly binder system consisting of lactose and tannin. The composition was optimized by systematically changing the lactose-tannin ratio. A slip casting route was developed for the manufacture of L–T-based compact cylinders. All of the obtained results can be used for further development of the Al_2O_3-C based filter materials.

Acknowledgements The studies were carried out with financial support from the Deutsche Forschungsgemeinschaft (DFG, German Research Foundation) within Collaborative Research Center CRC 920, subproject C02, Project-ID 169148856. The authors gratefully acknowledge the production and testing of some of the materials by Y. Ranglack-Klemm and Dr. J. Solarek, Institute of Materials Engineering, as well as the support from the colleagues at the Institutes of Ceramics, Refractories and Composite Materials as well as Materials Engineering and all other colleagues for their valuable contributions.

References

1. K. Schwartzwalder, A.V. Somers, General motors corporation, US Patent, US3090094, 21 May 1963
2. M.J. Pryor, T.J. Gray, Swiss aluminium limited, US Patent, US3947363, 30 March, 1976
3. J.C. Yarwood, J.E. Dore, R.K. Preuss, Swiss aluminium limited, US Patent, US3962081, 8 June, 1976
4. R.A. Olson III., L.C.B. Martins, Adv. Eng. Mater. **7**, 187 (2005). https://doi.org/10.1002/adem.200500021
5. V. Roungos, C.G. Aneziris, Refractories Worldforum **3**, 94 (2011)
6. M. Emmel, C.G. Aneziris, Ceram. Int. **38**, 5165 (2012). https://doi.org/10.1016/j.ceramint.2012.03.022
7. Y. Klemm, H. Biermann, C.G. Aneziris, Ceram. Int. **39**, 6695 (2013). https://doi.org/10.1016/j.ceramint.2013.01.108
8. Y. Klemm, H. Biermann, C. Aneziris, Adv. Eng. Mater. **15**, 1224 (2013). https://doi.org/10.1002/adem.201300159
9. Y. Klemm, H. Biermann, C.G. Aneziris, *Proceedings of the UNITECR 2013* (John Wiley & Sons, Inc, Hoboken, 2014)
10. I.J. Holland, US Patent, US3097930, 16 July, 1963
11. T. Wetzig, A. Baaske, S. Karrasch, N. Brachhold, M. Rudolph, C.G. Aneziris, Ceram. Int. **44**, 23024 (2018). https://doi.org/10.1002/adem.201900657
12. Y. Ranglack-Klemm, E. Storti, C. G. Aneziris, H. Biermann, Adv. Eng. Mater. **22**, 1900423 (2020). https://doi.org/10.1002/adem.201900423
13. X. Wu, Y. Ranglack-Klemm, J. Hubálková, J. Solarek, C.G. Aneziris, A. Weidner, H. Biermann, Ceram. Int. **47**, 3920 (2021). https://doi.org/10.1016/j.ceramint.2020.09.255
14. J. Solarek, C. Bachmann, Y. Klemm, C.G. Aneziris, H. Biermann, J. Am. Ceram. Soc. **99**, 1390 (2016). https://doi.org/10.1111/jace.14070
15. J. Solarek, C. Himcinschi, Y. Klemm, C.G. Aneziris, H. Biermann, Carbon **122**, 141 (2017). https://doi.org/10.1016/j.carbon.2017.06.041
16. J. Solarek, Dissertation, TU Bergakademie Freiberg, 2019
17. X. Wu, Y. Ranglack-Klemm, E. Storti, S. Dudczig, C.G. Aneziris, A. Weidner, H. Biermann, Adv. Eng. Mat. **24**, 2100642 (2022). https://doi.org/10.1002/adem.202100642
18. X. Wu, T. Wetzig, C.G. Aneziris, A. Weidner, H. Biermann, Adv. Eng. Mat. **24**, 2100613 (2022). https://doi.org/10.1002/adem.202100613
19. K.K. Kappmeyer, D.H. Hubble, *In High Temperature Oxides Part I – Magnesia, Lime, and Chrome Refractories* (Academic Press, New York, 1970)
20. Coal Tars and Coal-Tar Pitches, in: Report on Carcinogens, 14. Ed., National Institute of Environmental Health and Safety (2016)
21. Verordnung (EG) Nr. 1907/2006 (REACH), Registration, Evaluation, Authorisation and Restriction of Chemicals (2006)
22. E.M.M. Ewais, Carbon based refractories. J. Ceram. Soc. Japan **112**, 517 (2004). https://doi.org/10.2109/jcersj.112.517

23. Phenol, in: Hazardous Substance Fact Sheet, 2. Ed., New Jersey Department of Health (2015)
24. E. Guéguen, C.G. Aneziris, C. Biermann, German Patent, DE102016100083 AI
25. C. Biermann, Dissertation TU Bergakademie Freiberg (2016)
26. C. Himcinschi, C. Biermann, E. Storti, B. Dietrich, G. Wolf, J. Kortus, C.G. Aneziris, J. Eur. Ceram. Soc. **38**, 5580 (2018). https://doi.org/10.1016/j.jeurceramsoc.2018.08.029
27. J.A. Halt, S.K. Kawatra, Mining. Metallurgy & Exploration **31**, 73 (2014). https://doi.org/10.1007/BF03402417
28. A. Arbenz, L. Avérous, Green Chem. **17**, 2626 (2015). https://doi.org/10.1039/c5gc00282f
29. X. Wu, A. Weidner, C.G. Aneziris, H. Biermann, Ceram. Int. **48**, 148 (2022). https://doi.org/10.1016/j.ceramint.2021.09.090
30. X. Wu, A. Weidner, C.G. Aneziris, H. Biermann, Ceram. Int. **49**, 3140 (2023). https://doi.org/10.1016/j.ceramint.2022.12.192
31. G. Tondi, Polymers **9**, 223 (2017). https://doi.org/10.3390/polym9060223
32. A. Pizzi, P. Tekely, J. App. Polym. Sci. **56**, 1645 (1995). https://doi.org/10.1002/app.1995.070561215
33. H. Zielke, T. Wetzig, C. Himcinschi, M. Abendroth, M. Kuna, C.G. Aneziris, Carbon **159**, 324 (2020). https://doi.org/10.1016/j.carbon.2019.12.042
34. Z.A. Munir, U. Anselmi-Tamburini, M. Ohyanagi, J. Mater. Sci. **41**, 763 (2006). https://doi.org/10.1007/s10853-006-6555-2
35. O. Guillon, J. Gonzalez-Julian, B. Dargatz, T. Kessel, G. Schierning, J. Räthel, M. Hermann, Adv. Eng. Mater. **16**, 830 (2014). https://doi.org/10.1002/adem.201300409